Hypersonic Glide Vehicle Trajectory Design using Constrained Energy Maneuverability

Sam A. Jaeger* and Maziar S. Hemati †
University of Minnesota - Twin Cities, Minneapolis, Minnesota, 55455, U.S.A.

This paper presents a method that enables the rapid generation of physically relevant trajectories for a hypersonic glide vehicle (HGV). The method uses the concept of energy maneuverability (EM), whereby a set of energy differential equations are solved to generate a trajectory that is also constrained by the lifting capabilities of the trimmed HGV. Constrained EM trajectories are ensured to be dynamically feasible because they encode information about trim, the vehicle's energy state, and the equations of motion. EM trajectories can be computed rapidly and are well suited for initial vehicle design studies. A generic hypersonic glide vehicle developed at the University of Minnesota is used for the trajectory study. A high fidelity aerodynamic database generated from computational fluid dynamics is used to design and simulate trajectories. Heat, acceleration, aerodynamic loads are analyzed for the various trajectories computed. Additionally, transient temperature is computed using a lumped thermal mass model in the vehicle's nose. Trajectories designed using the proposed constrained EM approach are shown to alleviate the effects of skipping associated with unguided trajectories operating at high lift to drag ratios.

I. Introduction

Constructing physically relevant trajectories is a crucial step in the design process of hypersonic vehicles: mission design, vehicle design, and flight control design all depend on a nominal reference trajectory. These trajectories are often difficult to construct in hypersonics applications because the flight dynamics have nonlinearities that cannot be neglected, including from variable density atmosphere and spherical Earth effects. In this paper, we propose a constrained energy maneuverability method for rapid design of physically relevant trajectories for a hypersonic glide vehicle (HGV). We demonstrate the approach on a class of longitudinal trajectories for an HGV designed at the University of Minnesota [1]. These trajectories are computed using standard computational tools and can be used as a linearization trajectory for control algorithms or an initial guess for more sophisticated trajectory optimization methods.

Hypersonic trajectories can generally be classified into lifting and ballistic. Ballistic trajectories have the property of operating at low lift-to-drag (C_L/C_D) ratios and large flight path angles (γ) that do not vary significantly with time (i.e., $\dot{\gamma} \approx 0$). HGVs have much higher lift to drag (C_L/C_D) ratios compared to reentry capsules or ballistic warheads which follow ballistic trajectories. This allows HGVs to fly lifting trajectories that have much richer dynamics. Two characteristic maneuvers of lifting trajectories include a steady glide and a skip. Steady glide is similar to ballistic trajectories as the rate of change of the flight path angle stays close to zero for the majority of trajectory. A skip, on the other hand, is a dynamic maneuver where the vehicle enters the maneuver at a high C_L/C_D ratio, flight path angle, and velocity. Due to the variable atmosphere, the vehicle generates increasing lift as altitude decreases and then is eventually ejected back to higher altitude where the atmospheric density is much lower. These skips that appear as "phugoiding" create high loads on the vehicle and have high rates of energy dissipation. As a result, designing trajectories that alleviate skipping is often desirable. For reentry vehicles, skipping can eject vehicles back into orbit if the flight path angle and entry velocity are too high. Too low of an initial flight path angle and the vehicle could burn up. These two bounds correspond to the "entry corridor" [2]. Ballistic, glide, and skip trajectories are studied analytically in [3].

Previous work in this field have developed various approaches to designing trajectories ranging from analytical to optimization based approaches. These approaches are designed for atmospheric reentry problems and do not directly design a time varying energy state. Common assumptions in these methods include constant dynamic pressure, flat Earth, and a quasi-equilibrium glide, [4–6]. The benefit of using a dynamic pressure constraint is that an analytical relation can be made between altitude and velocity when using an exponential atmospheric model for density. Using a flat Earth model eliminates a source of nonlinearity in the equations of motion. However, for vehicles operating at high

*Graduate Student, Department of Aerospace Engineering and Mechanics, 110 Union Street SE, and AIAA Student Member (977106).
†Associate Professor, Department of Aerospace Engineering and Mechanics, 110 Union Street SE, and AIAA Associate Fellow.

altitudes and velocities this may not be a good assumption. Similarly, a quasi-equilibrium glide constraint simplifies the equations of motion for the flight path angle by assuming that lift approximately equals weight.

Other approaches design a drag profile and also analyze the trajectory via vehicle energy [7]. However, these approaches are designed for atmospheric reentry trajectories and also do not design the energy state directly. Several papers work to design α profiles based on best range and/or load constraints [8, 9]. A heating load constraint can also be used to to design trajectories [10]. Finally, work completed by [11] uses indirect methods to design trajectories for a minimum terminal energy of a boost-glide reconnaissance vehicle.

This paper works to directly design a time varying energy state of the vehicle to obtain a gliding guidance trajectory without applying a dynamic pressure constraint. A similar constraint to quasi-equilibrium-glide will be introduced in this paper that helps enforce the lifting capability of the vehicle.

A. Specific Energy and Energy Maneuverability

The work presented in this paper uses the concept of specific energy by [12] and [13]. This functional form of energy formulated originally for solving aircraft performance problems as well as codifying fighter aircraft tactics. The vehicle's energy can be defined as the sum of kinetic and potential energies:

$$E = mgh + \frac{1}{2}mV^2. \tag{1}$$

Where m is mass, g is the acceleration due to gravity, h is the vehicles altitude, and V is the vehicles velocity. By dividing by weight (mg), specific energy (energy per pound of vehicle) can be defined:

$$E_s = h + \frac{V^2}{2g}. \tag{2}$$

This specific energy quantity relates kinematic quantities to a scalar energy state of the vehicle and has units of length (this is a similar quantity to head height in fluid mechanics). The derivative can be taken with respect to time which becomes:

$$P_s = \dot{E}_s = \frac{-DV}{mg} = -\frac{\rho V^3 C_D}{2W_s}. \tag{3}$$

P_s denotes the specific energy rate of loss and was coined as "energy maneuverability" by Boyd [13]. W_s denotes the wing loading which is defined as the vehicle weight divided by the wing area (W/S_w). For a hypersonic glide vehicle, P_s will always be strictly negative as the vehicle is always loosing energy via drag. This work will focus on generating a full vehicle state trajectory from a specified E_s profile.

B. Equations of Motion

Because energy state of the vehicle can be completely described by longitudinal quantities, h and V, this work will study longitudinal flight. The longitudinal equations of motion for a hypersonic glide vehicle are shown in Equation 4. These equations of motion are derived and are studied in detail in [2, 3].

$$\begin{Bmatrix} \dot{h} \\ \dot{s} \\ \dot{V} \\ \dot{\gamma} \\ \dot{\theta} \\ \dot{q} \end{Bmatrix} = \begin{Bmatrix} V \sin\gamma \\ V \cos\gamma \\ -\frac{\rho V^2 S_w C_D}{2m} - g \sin\gamma \\ \frac{\rho V S_w C_L}{2m} - \left(\frac{g}{V} - \frac{V}{R_0 + h}\right)\cos\gamma \\ q \\ \frac{1}{2}\rho V^2 S_w \bar{c} C_m / I_{yy} \end{Bmatrix}. \tag{4}$$

Where s is downrange, γ is the flight path angle, θ is the pitch attitude, and q is the pitch rate. Additionally, S_w is the vehicle's wing reference area, $\bar{c}$ is the vehicles mean aerodynamic chord, C_L, C_D, C_m are the vehicle's lift, drag and pitching moment coefficient respectively, R_0 is the radius of the Earth, and I_{yy} is the moment of inertia about the pitch axis of the vehicle. In addition to these equations an exponential atmosphere model is applied:

$$\rho = \rho_0 e^{(-\beta h)}. \tag{5}$$

Where ρ_0 is the density at sea level and β is an atmospheric density lapse rate. Both of these are assumed to be constant. These equations assume a constant acceleration due to gravity and a spherical Earth. Finally, the altitude and downrange kinematics can be described faithfully by $V \sin\gamma$ and $V \cos\gamma$. Vehicle properties and aerodynamics are presented in the next section.

C. G2 Geometry and Vehicle Properties

This paper uses the G2 vehicle geometry developed at the University of Minnesota as a numerical example [1]. A three dimensional render of the G2 can be seen in Figure 1.

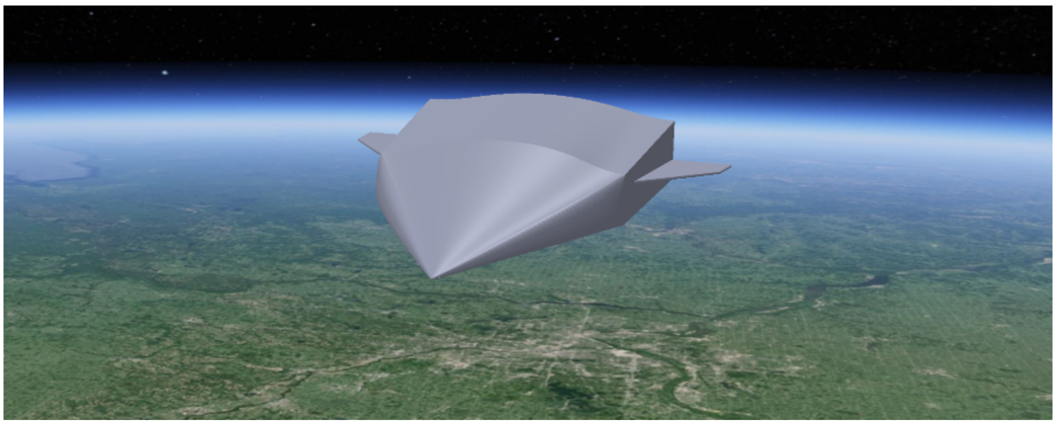

Fig. 1 G2 vehicle geometry flying in the upper atmosphere above Minneapolis, Minnesota.

Mass and geometry properties of the G2 vehicle were set to be $m = 1000\ kg$, $I_{yy} = 429.3\ kg - m^2$, $S_w = 4.4\ m^2$, $\bar{c} = 3.6\ m$, $x_{cg} = 2.04\ m$ aft from the nose of the vehicle. I_{yy} was selected using historical high performance aircraft inertia data from [14]. The x_{cg} location was selected to provide static stability ($\frac{\partial C_m}{\partial \alpha} < 0$) in addition to static trim ($C_m = 0$) for an acceptable range of α.

D. G2 Aerodynamics

A high fidelity database was constructed in [1] using high fidelity computational fluid dynamics (CFD). US3D was used as the CFD solver and a laminar boundary layer was assumed. Steady solutions of C_L, C_D, C_m were computed for a range of α, δ, V, and h. For this work, the CFD data at $V = 2500\ m/s$ and $h = 35\ km$ was used to simplify the functional dependency of the aerodynamic coefficients. A spline interpolation lookup table is used for computing aerodynamic coefficients for simulations and trajectory design. Newtonian aerodynamics was originally used to generate the aerodynamic database, however it was found that pitching moment data generated from Newtonian aerodynamics was not accurate. Aerodynamic data from CFD for C_L/C_D, C_D, and C_m are shown in Figure 2.

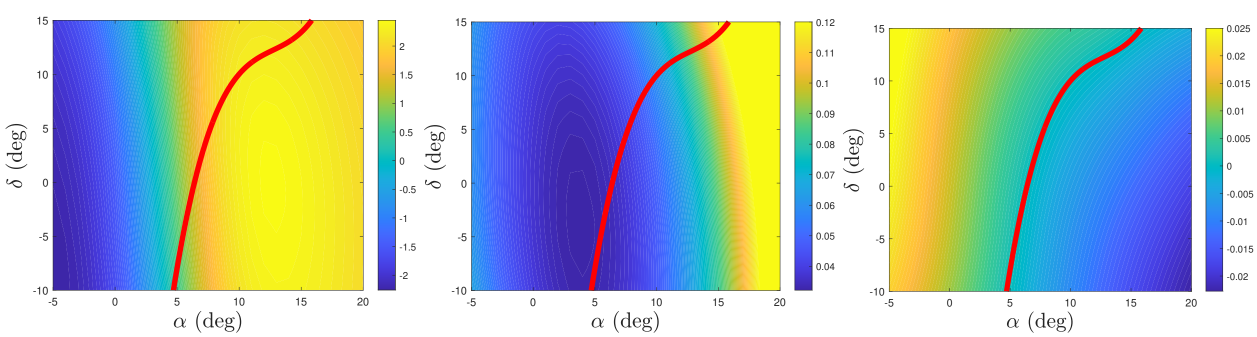

(a) C_L/C_D **(b)** C_D **(c)** C_m **at** $x_{cg} = 2.04\ m$.

Fig. 2 Aerodynamic properties for α and δ combinations at $V = 2500 m/s$, $h = 35 km$. The red line is a cubic fitted polynomial for trim values of $C_m = 0$ at $x_{cg} = 2.04\ m$ behind the nose.

Pitching moment is a critical quantity for finding suitable trajectories in that the vehicle must be balanced in order to trim or be close to trim. For the purposes of this work, trim is defined at $C_m = 0$. This condition was found for combinations of α, δ and a cubic polynomial was fitted to these points. This cubic polynomial is shown as a red line in Figure 2. Trajectories can be designed under a trim assumption ($C_m = 0$) which reduces the aerodynamic dependency from α and δ to just α. Note that the absolute maximum C_L/C_D and minimum C_D do not correspond to a trim condition for the selected x_{cg} location. Values of trimmed C_D and C_L/C_D for all of the CFD data generated are plotted in Figures 3a and 2a. Additionally, cubic polynomials for the α, δ trim conditions are plotted in Figure 3.

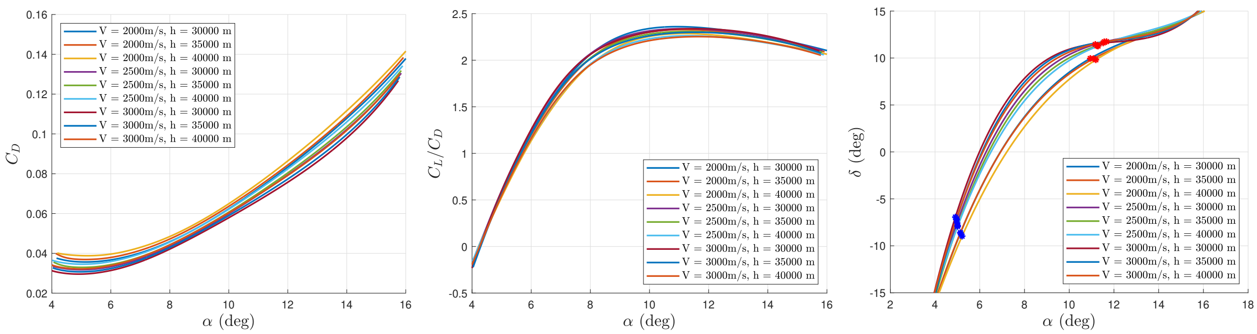

(a) C_D for trim conditions. **(b) C_L/C_D for trim conditions.** **(c) α vs δ curves for trim conditions.**

Fig. 3 Aerodynamic properties for trim conditions $C_m = 0$. Blue dots correspond to values of minimum C_D, red dot correspond to values of maximum C_L/C_D.

The trim condition that corresponds to the minimum C_D as well as the maximum C_L/C_D is explored in synthesizing trajectories. As shown in Figure 3 the angle of attack corresponding to the maximum C_L/C_D condition as well as the minimum C_D condition does not vary significantly between altitude and velocity datasets. This justifies using a single altitude-velocity CFD dataset for trajectory design.

II. Energy Based Trajectory Design

This section presents rules and constraints for generating energy profiles.

A. Functional Constraints

Energy and energy maneuverability are scalar functions of finite time $E_s \in \mathbb{R}, P_s \in \mathbb{R}$ with the final time (t_f) defined when altitude is zero. Four basic rules must be followed when generating energy trajectories:

1) E_s must always be positive for the trajectory time range: $E_s(t) > 0, t \in [0, t_f]$.
2) P_s must always be negative for the trajectory time range: $P_s(t) < 0, t \in [0, t_f]$.
3) E_s, P_s must match kinematics: $\dot{P}_s$ must match equations of motion.
4) E_s, P_s must be continuous.

Having a positive energy enforces trajectories with positive altitudes. Additionally, a strictly negative P_s reflects the fact that the vehicle is always loosing energy and thus E_s is a monotonically decreasing value between $t = [0, t_f]$. The energy state matching the kinematics allows dynamic inversion to be utilized for computing the full state history. Finally, designing continuous in time trajectories helps to generate a physically meaningful solution.

B. Constrained Energy Maneuverability

The third rule of constructing energy trajectories essentially enforces that the energy state reflects the equations of motion in 4. Arbitrary energy profiles may not be dynamically feasible because the vehicle cannot produce enough lift for a given drag coefficient and trim state. In order to find both a dynamically and energy feasible trajectory, energy must be constrained. This can be done by taking the derivative of energy maneuverability:

$$\dot{P}_s = \frac{-1}{W}\left(\dot{D}V + D\dot{V}\right) = \frac{-\bar{q}C_D}{W_s}\left(-\beta V\dot{h} + 3\dot{V} + \frac{V}{C_D}\dot{C}_D\right). \tag{6}$$

Equation 6 can be expanded and simplified:

$$\dot{P}_s = \frac{\bar{q}C_D}{W_s}\left(\left(\beta V^2 + 3g\right)\sin\gamma + 3\bar{q}C_D\frac{g}{W_s} - \frac{V}{C_D}\dot{C}_D\right). \tag{7}$$

Where $\bar{q}$ is the dynamic pressure. Note that the dependence of γ cannot be eliminated in Equation 7. Thus, Equation 7 must be coupled with the $\dot{\gamma}$ equation of motion which encodes information about the lifting capability of the vehicle. $\dot{\gamma}$ can be rewritten in terms of energy and energy maneuverability:

$$\dot{\gamma} = \frac{-gP_s}{V^2}\left(\frac{C_L}{C_D}\right) + \left(\frac{V}{R_0 + E_s - \frac{V^2}{2g}} - \frac{g}{V}\right)\cos\gamma. \tag{8}$$

Equations 7 and 8 can be integrated in time to find an energy profile. In this work, trajectories with $\dot{C}_D = 0$ will only be considered which corresponds to a constant α profile.

Another constraint that can be introduced is a specified $\dot{\gamma}$. This constraint is similar in nature to a quasi-equilibrium glide condition [5]. For this type of trajectory, the γ equation of motion can be rewritten in terms of an energy maneuverability constraint:

$$P_s = \left(\frac{V^2}{g(C_L/C_D)}\right)\left(\left(\frac{V}{R_0 + E_s - \frac{V^2}{2g}} - \frac{g}{V}\right)\cos\gamma - \dot{\gamma}\right). \tag{9}$$

Equation 9 can be integrated in time to find an energy profile E_s for a specified $\dot{\gamma}$. Arbitrary $\dot{\gamma}$ cannot be specified for an initial energy state. For an initial energy state (E_{s_0}, P_{s_0}), there is a unique α that satisfies 9 at the initial energy state. Thus, 9 can be solved for C_L/C_D and the resulting α can be found from a fitted C_L/C_D curve as in Figure 3b. For the HGV vehicle used in this paper, $\dot{\gamma}$ is constrained trimmable C_L/C_D over the ranges $-0.17 < \dot{\gamma} \leq 0$ deg$/s$. Additionally, a specified constant $\dot{\gamma}$ over a finite time domain requires $\dot{\gamma} \leq 0$. For the special case of $\dot{\gamma} = 0$ the flight path angle must be < 0 as the HGV does not have thrust.

III. Constructing State Trajectories via Dynamic Inversion

This section depicts how to construct the full state of the vehicle once E_s and P_s trajectories are designed. In order to do this, an α profile must be designed. This section overviews three different α profile designs as well as the general algorithm for constructing the state trajectory.

A. α Profile Design

One method of historically generating guidance trajectories is to design a drag profile. In this same spirit, α and thus C_D, C_L/C_D profiles are designed. Within this, three different α profiles are studied:

1) Minimum C_D.
2) Maximum C_L/C_D.
3) Specified $\dot{\gamma}$.

From the designed α profile, nominal δ deflections can also be computed by assuming a trim condition throughout the trajectory. This will be a good assumption for trajectories with small pitch rates. Other trajectory optimization methods could be employed to generate time varying α profiles which would correspond to $\dot{C}_D \neq 0$.

B. Dynamic Inversion

To compute a set of reference states from energy and α profiles, dynamic inversion is used. The first step is to use Equations 2 and 3 as well as the exponential atmosphere to compute velocity. These three equations can be put into the form:

$$V^3 \exp\frac{\beta V^2}{2g} = -\frac{2P_s W_s \exp\beta E_s}{\rho_0 C_D} = K(t). \tag{10}$$

Equation 10 can be solved using a nonlinear root finder such as Brandt's method. Once velocity is solved for, the rest of the state can also be found. Algorithm 1 overviews the steps to construct a state space trajectory for a given E_s, P_s, C_D, γ.

Algorithm 1 Dynamic Inversion from an Energy profile

Given: $E_s(t)$, $\alpha(t)$, $P_s(t)$, $C_D(t)$, $\gamma(t)$ ▷ Must satisfy energy rules.
Calculate: $K(t) = -\frac{2P_s(t)W_s \exp[\beta E_s(t)]}{\rho_0 C_D(t)}$
for $t_0 : t_f$ **do** ▷ Brant's method works well. Solution will be unique.
  Solve: $0 = K(t) - V^3 \exp\frac{\beta V^2}{2g}$ for V via nonlinear root solver.
end for
Calculate: $h(t) = E_s(t) - \frac{V(t)^2}{2g}$
Calculate: $\theta(t) = \gamma(t) + \alpha(t)$
Calculate: $q(t)$ via finite differencing of θ. ▷ First order works well with a sufficiently small time step.
Calculate: $s(t)$ by numerically integrating $\dot{s} = V\cos\gamma$ ▷ Trapezoidal integration has shown to be sufficient.

IV. Trajectories and Loads Analysis

The initial conditions are the same for all of the trajectories computed except for the angle of attack. The initial attitude (θ_0) was varied to match the α required for the specific C_D and C_L/C_D for the trajectory. The initial conditions for the trajectories were set to $V_0 = 3\ km/s$, $h_0 = 40\ km$, $\gamma_0 = -2$ deg, $q_0 = 0$ deg$/s$. This corresponds to an initial energy state $E_{s_0} = 4.9872 * 10^5\ m$.

A. Trajectories

Altitude versus downrange is computed and is shown in Figure 4. Note that the maximum C_L/C_D and minimum C_D energy trajectories closely approximate the open loop trajectories. This verifies the method of designing trajectories via an energy state and reflects the fact the energy designed trajectories eliminate the short period dynamics. Eliminating the short period dynamics assumes that a controller can perfectly regulate angle of attack.

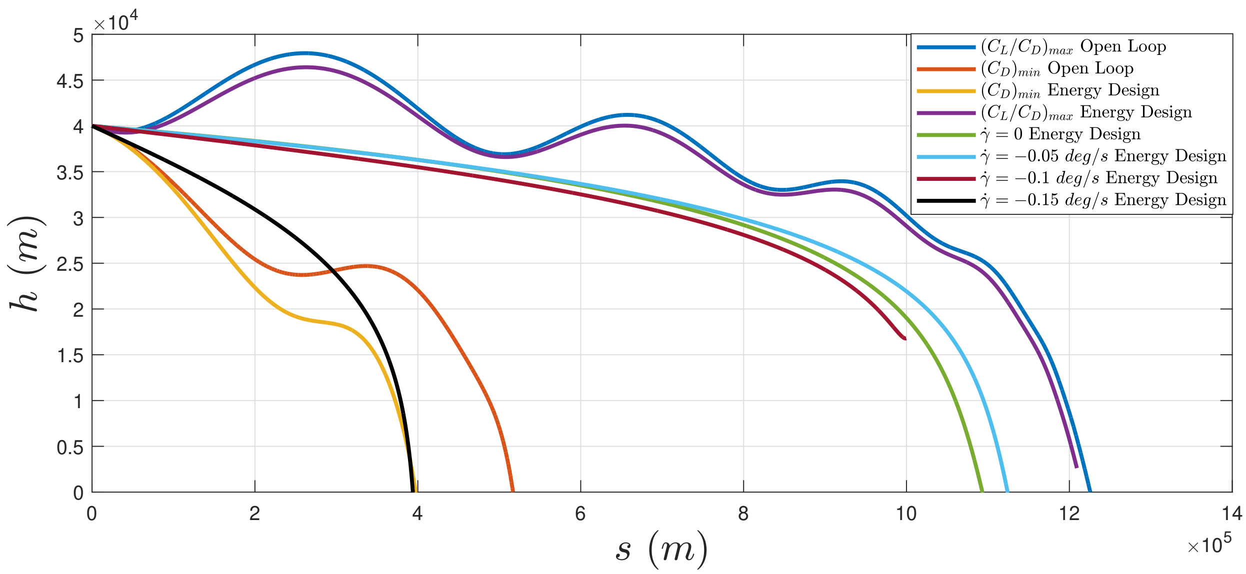

Fig. 4 Altitude versus downrange for computed trajectories.

In addition to altitude versus downrange, velocity, flight path angle, pitch attitude and pitch rate are shown in Figure 5.

Velocity is shown to follow the same basic trajectory for the majority of the specified $\dot{\gamma}$ cases as well as maximum C_L/C_D cases. Additionally, γ for the maximum C_L/C_D cases are shown to oscillate around the $\dot{\gamma} = 0$ case. The pitch attitude slowly pitches down throughout the trajectory for all of the cases except for the $\dot{\gamma} = 0$ case. Finally, the short period dynamics appear in the pitch rate for the open loop trajectories and the energy designed trajectories smooth these dynamics out.

Energy and EM time histories are plotted in Figure 6.

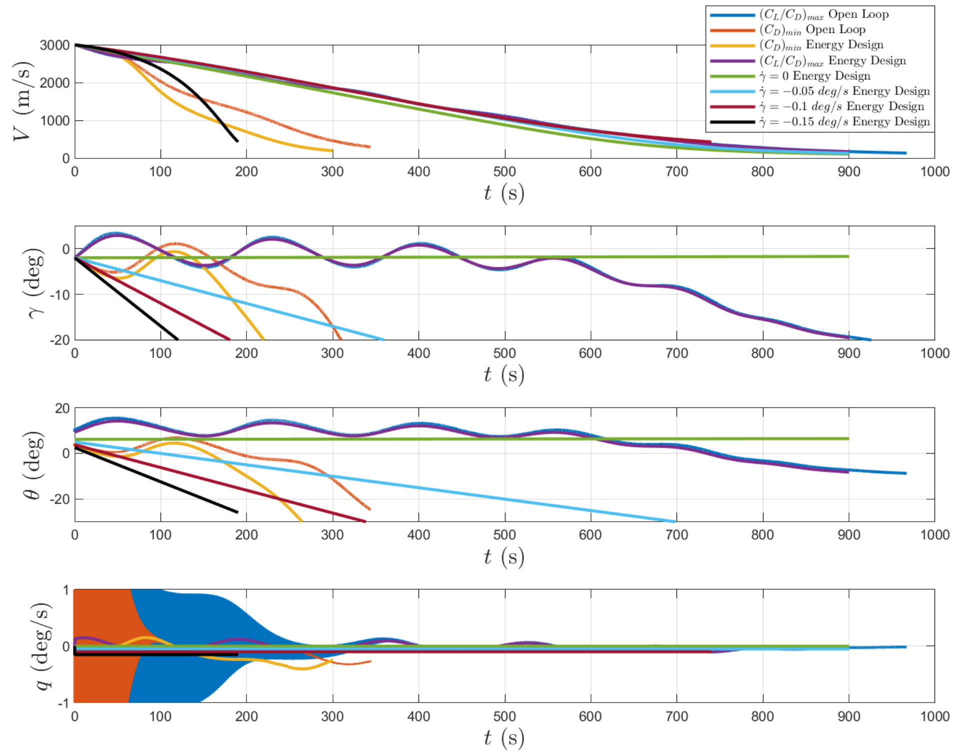

Fig. 5 State time histories for computed trajectories.

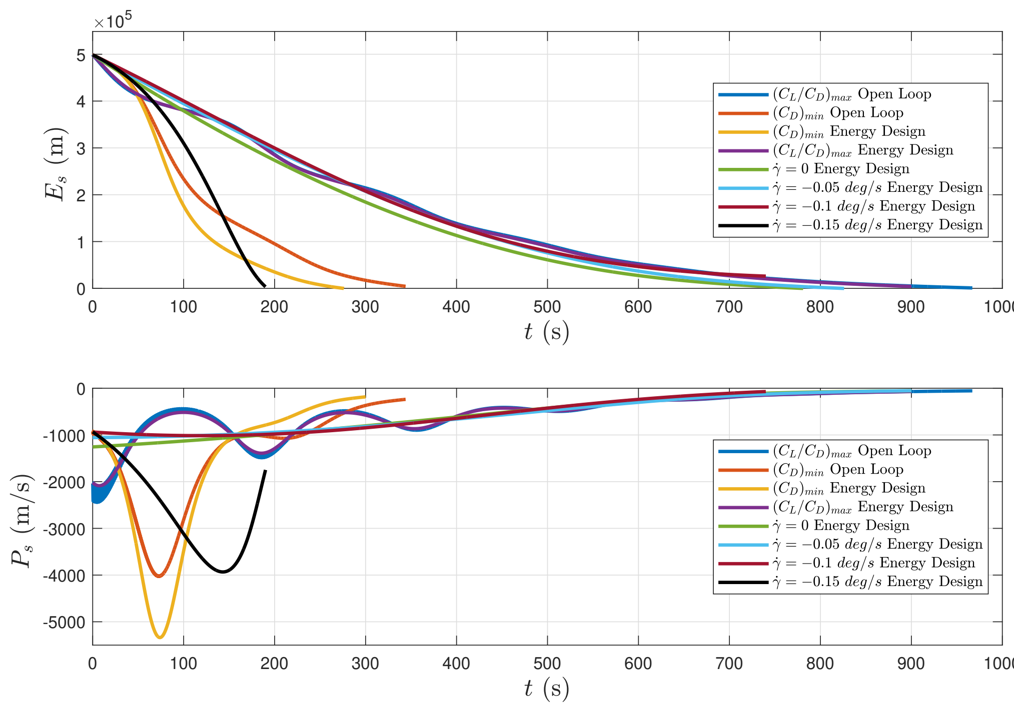

Fig. 6 Energy and energy maneuverability time histories for computed trajectories.

As shown in the EM time history, skipping is associated with high rates of energy loss. Additionally, the short period dynamics in the open loop trajectories propagate into the EM time histories. Finally, E_s and P_s time histories have the property of asymptotically approaching zero. The two quantities comprising energy (V, h) are also plotted in Figure 7.

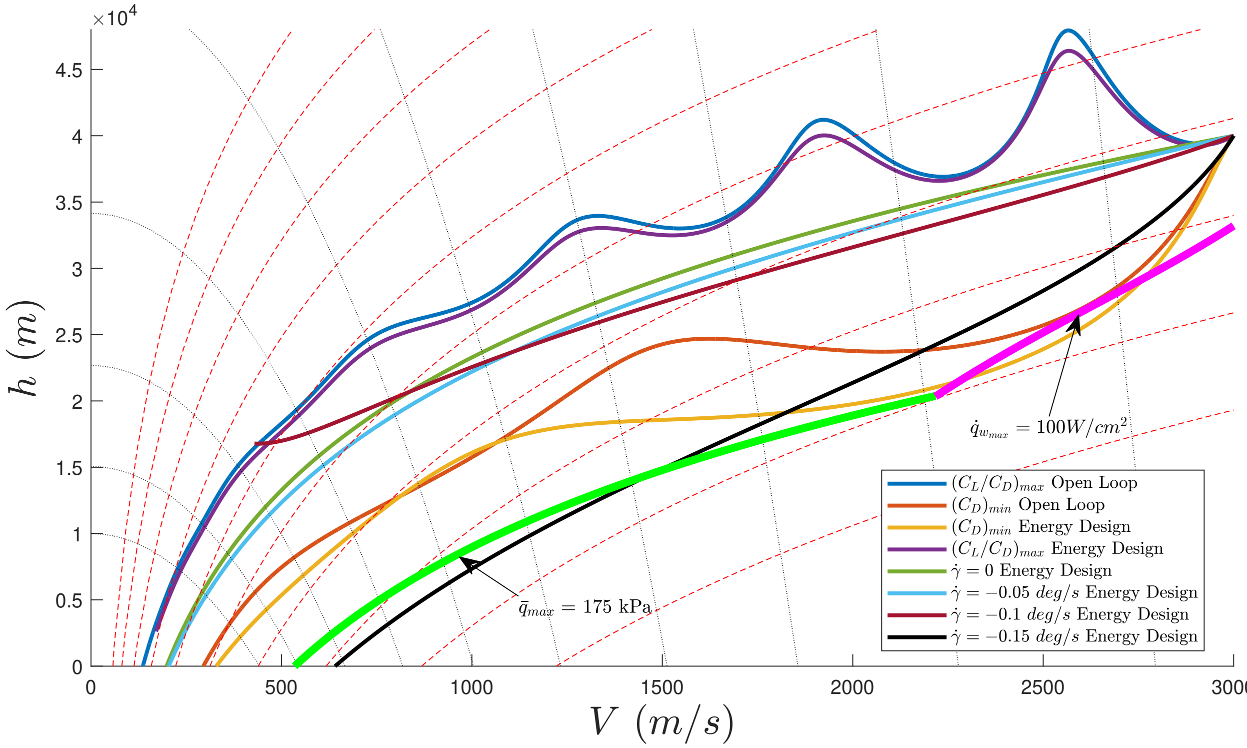

Fig. 7 Altitude versus velocity trajectories. Black dotted lines denote trajectories of constant energy. Red dashed lines denote trajectories with constant energy loss. Additionally, maximum dynamic pressure (175 kPa) and heat flux constraints (100 W/cm^2) are plotted with thick green and magenta lines respectively.

The trajectories in altitude-velocity space all approach the origin but have different impact velocities. Specified $\dot{\gamma}$ trajectories have a relatively constant rate of energy loss while the skipping trajectories have varying rates of energy loss. Maximum heat flux and dynamic pressure constraints are violated for the minimum C_D and $\dot{\gamma} = -0.15$ deg$/s$ trajectories. These constraints are often the lower bound of the "entry corridor" used for mission design [2]. Note that constant heat flux and dynamic pressure constrained trajectories do not have constant energy loss and are fundamentally different trajectories than energy designed trajectories. The $\dot{\gamma} = -0.1\ deg/s$ trajectory is a case where trajectory can become overconstrained. In this overconstrained case, the vehicle runs out of velocity at significant altitude while trying to maintain the required γ.

B. Loads

Three different loads are computed and compared for the trajectories. These include dynamic pressure ($\bar{q}$), total load factor (n), and heat flux ($\dot{q}_w$). Dynamic pressure is a measure of the aerodynamic load on the structure, load factor is a measure of the acceleration on the vehicle, and heat flux is a measure of the aerodynamic heating on the vehicle. Dynamic pressure and total load factor are defined as:

$$\bar{q} = \frac{1}{2}\rho V^2, \tag{11}$$

$$n = \frac{\sqrt{L^2 + D^2}}{W}. \tag{12}$$

Heat flux is computed by using a Van Driest model of the stagnation point on the vehicle [15]:

$$\dot{q}_w = \kappa Pr^{-0.6} \sqrt{\rho_e \mu_e} \frac{1}{\sqrt{R_n}} \left(\frac{2(P_e - P_1)}{\rho_e} \right)^{1/4} (h_{aw} - h_w). \tag{13}$$

In this model, the flow pass through a strong normal shock and then a laminar boundary layer equations are solved assuming a perfect gas. Thus, the subscripts e denote the boundary layer edge conditions or the flow conditions directly after the shock. Additionally, the w subscript denotes the wall conditions of the stagnation point on the vehicle. The stagnation point geometry is assumed to approximate a sphere and thus $\kappa = 0.763$. Pr is the Prandtl number and is set to 0.72 for air. ρ_e and μ_e is the density and the viscosity respectively of air at the boundary layer edge. μ_e is computed using Sutherland's law which computes viscosity as a function of temperature. R_n is the nose radius and is set to 0.2 m. P_e and P_1 are the pressure at the boundary layer edge and free stream conditions. h_w, h_{aw} correspond to enthalpies of the wall and adiabatic wall respectively which assume the wall to be at a constant temperature at 500 K. Heat flux was only computed for high supersonic conditions ($M > 3$) since the Van Driest model requires the freestream flow to be supersonic to compute post shock conditions and gains accuracy as hypersonic flow conditions are approached. [6] gives an approximate analytical relation for heat flux as $\dot{q}_w = k_q \sqrt{\rho} V^{3.15}$, however the k_q constant is dependent on vehicle configuration.

Time histories of dynamic pressure, acceleration, and heat flux are presented in Figure 8.

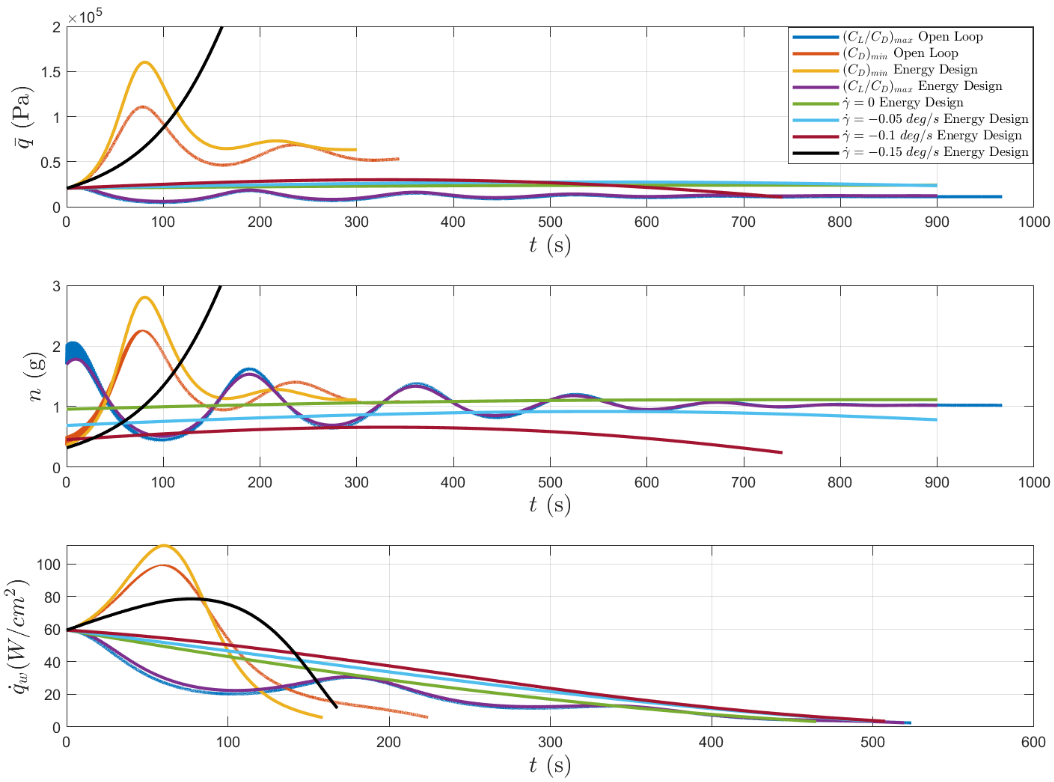

Fig. 8 Dynamic pressure ($\bar{q}$), total load factor (n), and heat flux at constant wall temperature ($\dot{q}_w$) loads for trajectories computed.

In addition to dynamic pressure, load factor, and heat flux with constant wall temperature, transient temperature was calculated using a lumped thermal mass model of inconel 625. This thermal model has Van Driest convective heat load along with an emissive radiation model. Combining these two models results in the following differential equation:

$$\frac{dT_w}{dt} c_n \rho_n \cancel{V}_n / A_n = \dot{q}_w - \dot{q}_{rad}. \tag{14}$$

Where c_n is the heat capacity of inconel (which is modeled as a quadratic function of temperature), ρ_n is the density of inconel, and V_n/A_n is the nose volume divided by the surface area exposed to the flow. This ratio of volume to area was approximated by a sphere that is cut by an angle, which reduces to $V_n/A_n = R_n/3$. Finally, $\dot{q}_{rad} = \sigma\epsilon(T_w^4 - T_\infty^4)$ where σ is the Stefan-Boltzmann Constant, $\epsilon = 0.8$ is the emissivity of the nose and T_∞ is the ambient (free stream) temperature. Using this transient temperature model, the differential equation is numerically integrated for each of the trajectories. The resulting temperature profiles are shown in Figure 9. As the trajectories velocities are reduce below Mach 3, the convective convective heat flux is set to zero as the Van Driest heating model looses accuracy.

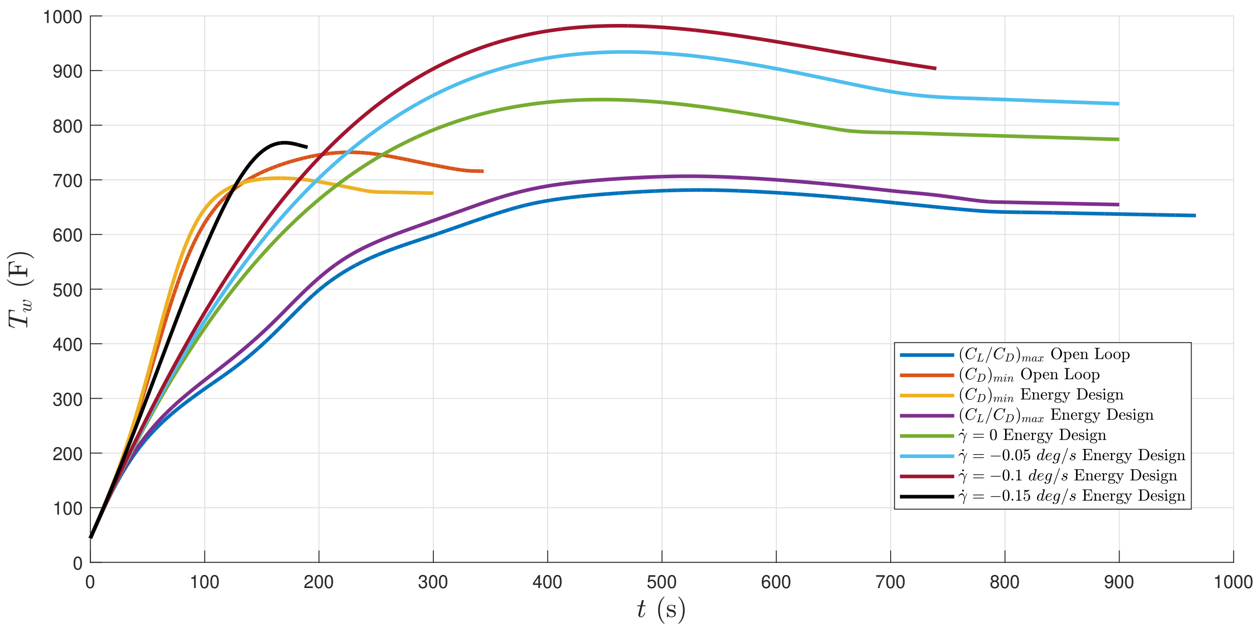

Fig. 9 Transient temperature time history for a lumped thermal mass in the vehicles nose with a convective heat flux load and radiative heat flux out. Initial temperature was set to 50 F.

As shown in Figures 8 and 9 the specified $\dot{\gamma}$ profiles reduce the peak load factor associated with skipping but has a higher heat flux and transient temperature. This is because the unguided skipping trajectory stays at higher altitudes where the air is less dense while the velocities are relatively high. Despite this, the calculated heat flux and transient temperature loads are well within the thermal capabilities of inconel. For reference, the maximum heat flux on the Space Shuttle was on the order of 30 W/cm^2 and on Apollo Command Module was on the order of 200 W/cm^2 [16].

While range is best for the open loop trajectory, the peak load factor is significantly higher compared to the energy designed $\dot{\gamma}$ trajectory. Additionally, the specified $\dot{\gamma}$ trajectories have an approximately constant dynamic pressure throughout their trajectories. This shows why a constant dynamic pressure constraint has historically been used to design these sorts of trajectories.

V. Conclusion

Longitudinal trajectories can be computed using a set of coupled differential equations for energy maneuverability and γ. A class of these trajectories are computed at a constant angle of attack for a specified $\dot{\gamma}$ profile using CFD results [1]. Trajectories designed by constrained EM are ensured to be dynamically feasible because they encode information about trim in addition to the equations of motion. EM trajectories can be computed rapidly and are well suited for initial vehicle design studies or as an initial guess for trajectory optimization methods. Future work will focus on extending the EM approach to out-of-plane trajectories, $\dot{C}_D \neq 0$, as well as integrated control law design, enabling analysis and design of a comprehensive set of HGV missions.

VI. Acknowledgments

This material is based upon work supported by the Air Force Office of Scientific Research under award number FA9550-22-1-0004.

References

[1] Williams, D., Bhattacharjee, D., Drayna, T. W., Bartkowicz, M., Hemati, M., and Candler, G. V., *Integrated Guidance and Control of Generic Hypersonic Glide Vehicles Using Computational Fluid Dynamics*, AIAA SCITECH, 2025. https://doi.org/10.2514/6.2025-0264.

[2] Vinh, N., Busemann, A., and Culp, R., *Hypersonic and Planetary Entry Flight Mechanics*, 1st ed., University of Michigan Press, 1980.

[3] Vinh, N. X., *Flight Mechanics of High-Performance Aircraft*, 1st ed., Cambridge., 1993, Chaps. 5,9,11.

[4] Kelly, H., Cliff, E., and Lutze, F., "Boost-glide range-optimal guidance," *AIAA Guidance and Control Conference*, 1981. https://doi.org/10.2514/6.1981-1781.

[5] Lu, P., "Asymptotic Analysis of Quasi-Equilibrium Glide in Lifting Entry Flight," *Journal of Guidance, Control, and Dynamics*, Vol. 29, No. 3, 2006, pp. 662–670. https://doi.org/10.2514/1.15789.

[6] Lu, P., "Entry Guidance: A Unified Method," *Journal of Guidance, Control, and Dynamics*, Vol. 37, No. 3, 2014, pp. 713–728. https://doi.org/10.2514/1.62605.

[7] Zhang, W., Chen, W., and Yu, W., "Entry Guidance for High-L/D Hypersonic Vehicle Based on Drag-vs-Energy Profile," *ISA Transactions*, Vol. 83, 2018, pp. 176–188. https://doi.org/https://doi.org/10.1016/j.isatra.2018.08.012.

[8] Palumbo, R., Morani, G., and Cicala, M., "Reentry Trajectory Optimization for Mission Analysis," *Journal of Spacecraft and Rockets*, Vol. 54, No. 1, 2017, pp. 331–336. https://doi.org/10.2514/1.A33465.

[9] Zhaoying, L., Rui, Z., and Yuxin, L., "Angle of Attack Operation Zone Analysis and Design for Lifting Entry," *28th International Congress of the Aeronautical Sciences*, 2012.

[10] Zimmerman, C., Dukeman, G., and Hanson, J., "Automated Method to Compute Orbital Reentry Trajectories with Heating Constraints," *Journal of Guidance, Control, and Dynamics*, Vol. 26, No. 4, 2003, pp. 523–529. https://doi.org/10.2514/2.5096.

[11] Grant, M. J., and Bolender, M. A., *Minimum Terminal Energy Optimizations of Hypersonic Vehicles Using Indirect Methods*, AIAA, 2015. https://doi.org/10.2514/6.2015-2402.

[12] Rutowski, E. S., "Energy Approach to the General Aircraft Performance Problem," *Journal of the Aeronautical Sciences*, Vol. 21, No. 3, 1954, p. 187–195. https://doi.org/10.2514/8.2956.

[13] Boyd, J., Christie, T., and Gibson, J., "Energy-Maneuverability," *United States Air Force Report*, 1966. URL https://www.archives.gov/files/declassification/iscap/pdf/2011-052-doc1.pdf.

[14] Phillips, W., *Mechanics of Flight*, 2nd ed., John Wiley Sons, Inc., Hoboken, New Jersey, 2010.

[15] Van Driest, E., "The Problem of Aerodynamic Heating," *IAS Confrence: Aerodynamic Heating*, 1956.

[16] Candler, G., "AEM 5247: Hypersonic Aerodynamics," Class Notes for Hypersonics, Spring 2024.